13 February 2026

New MnO2 electrode doped with Co2+ ions for a microfluidic biosensor for the detection of H2O2: formation, characterization, catalytic tests

Veronika Poltavets[1,2], Mirosław Krawczyk[1], Ganna Maslak[2], Martin Jönsson-Niedziółka[1]

1. Institute of Physical Chemistry of the Polish Academy of Sciences

2. Department of Biochemistry and Medical Chemistry, Dnipro State Medical University

Abstract

H_2O_2 serves as a vital signalling molecule within biological systems and presents potential as a disease biomarker. Consequently, the development of sensitive and accurate sensors for its measurement within microfluidic systems is of significant importance. This article focuses on the development of a working electrode for an electrochemical microfluidic system designed for the quantitative determination of hydrogen peroxide. Here, we show that a MnO_2-based catalytic material can be improved by adding Co^{2+} ions. By changing the Co^{2+} concentration, an electrode material with improved catalytic performance was formed. Amperometric measurements of catalytic activity show a substantial increase in sensitivity and an expanded range of H_2O_2 concentrations that can be quantified using the new electrode. The characteristics of the MnO_2-modified Co^{2+} electrode were thoroughly examined by SEM, XPS. The combination of previously accumulated material and new data offers insights into the underlying reasons for the high catalytic activity of MnO_2, supported by quantum-chemical calculations. This research lays the groundwork for a method utilising MnO_2 as a working electrode for detecting the concentration of H_2O_2 within a microfluidic cell. During experiments, a stopflow protocol is employed, enabling data collection from coulometric measurements of the electrochemical processes occurring on the electrode within a limited measurement timeframe.

Keywords

biosensor, electrodeposition, microfluidic system, managanese oxide, Co-doping

Posted on 13 February 2026 — CC-BY 4.0 — This is a preprint and has not been peer reviewed. Data may be preliminary. — https://doi.org/10.26434/chemrxiv.15000056/v1

New MnO_2 electrode doped with Co^{2+} ions for a microfluidic biosensor for the detection of H_2O_2: formation, characterization, catalytic tests.

Veronika Poltavets[*a,b], Mirosław Krawczyk[a], Ganna Maslak[b], Martin Jönsson-Niedziółka[*a]

[a] *Institute of Physical Chemistry of the Polish Academy of Sciences, Kasprzaka 44/52, 01-224 Warsaw, Poland.*

[b] *Department of Biochemistry and Medical Chemistry, Dnipro State Medical University, ul. Volodymyr Vernadsky 9, 49044 Dnipro, Ukraine.*

** Corresponding authors: martinj@ichf.edu.pl, verapolt9@gmail.com*

Abstract.

H_2O_2 serves as a vital signalling molecule within biological systems and presents potential as a disease biomarker. Consequently, the development of sensitive and accurate sensors for its measurement within microfluidic systems is of significant importance. This article focuses on the development of a working electrode for an electrochemical microfluidic system designed for the quantitative determination of hydrogen peroxide. Here, we show that a MnO_2-based catalytic material can be improved by adding Co^{2+} ions. By changing the Co^{2+} concentration, an electrode material with improved catalytic performance was formed. Amperometric measurements of catalytic activity show a substantial increase in sensitivity and an expanded range of H_2O_2 concentrations that can be quantified using the new electrode. The characteristics of the MnO_2-modified Co^{2+} electrode were thoroughly examined by SEM, XPS. The combination of previously accumulated material and new data offers insights into the underlying reasons for the high catalytic activity of MnO_2, supported by quantum-chemical calculations.

This research lays the groundwork for a method utilising MnO_2 as a working electrode for detecting the concentration of H_2O_2 within a microfluidic cell. During experiments, a stop-flow protocol is employed, enabling data collection from coulometric measurements of the electrochemical processes occurring on the electrode within a limited measurement timeframe.

Keywords: MnO_2-modified Co^{2+} electrode, biosensor, electrodeposition, microfluidic system.

1. Introduction.

Microfluidic systems as an analytical tool is a relatively recent development, but their use opens up great prospects [1–4] In the development of electrochemical microfluidic biosensors, the formation of the working electrodes is of utmost importance. These electrodes should provide sensitivity and selectivity to the sensor, but another important characteristic, especially in microfluidic systems is mechanical strength [5–7]. Therefore, electrodes with a catalyst layer are developed individually for specific analytes. The aim of this research is to develop a microfluidic biosensor for the determination of H_2O_2 in biological samples. Such sensors are of crucial importance and in high demand for a great number of applications. H_2O_2

is an anchor substance in the body's antioxidant system: peroxide compounds are intermediates or end products in almost all transformations [8,9]. Consequently, H_2O_2 can be used as a marker in biosensors for studying cancer tissue [10–14], diseases of various organs [15–18], etc. In Ukraine, since the beginning of the war, such studies are unfortunately in high demand, in such topics as the influence of polytrauma on the development of oxidative stress in people exposed to blast injuries.

In most studies, Au nanoparticles are used as a catalyst for the detection of H_2O[19–23], and the much cheaper MnO_2 (a specific catalyst for the decomposition of H_2O_2) is used much less frequently [24,25]. In our previous work, we developed an electrode that performed very well for glucose detection in microfluidic systems. This electrode was based on MnO_2 electrochemically deposited on the surface of ITO under conditions selected to exhibit maximum catalytic properties for high selectivity and sensitivity for hydrogen peroxide detection. In this study, we aim to improve the catalytic properties of MnO_2 by doping the oxide with Co^{2+} ions. The method of oxide doping is quite widespread [26–28], but despite this, there are only a few works on MnO_2 doping with cobalt ions [29,30], although one might have expected otherwise since the cobalt atom is very close in size to the manganese atom.

Investigating the reasons for the influence of doping on the properties of MnO_2 is also of interest. Most studies agree that doping affects defects in the crystal lattice of MnO_2 [31]. We will try to consider this effect from the point of view of changes in the oxygen-containing compounds in the sediment composition compared to pure MnO_2. To do this, we use XPS, SEM, and quantum chemical modelling to analyse a set of electrodes characterised by different contents of Co^{2+} ions.

The final part of this research is the creation of a microfluidic chip where the developed electrode was utilised to determine H_2O_2 concentrations.

2. Experimental.

2.1. Reagents and chemicals.

All materials and chemicals were purchased commercially and used in the form in which they were received. Manganese sulphate, cobalt sulphate and sodium sulphate for electrolytes preparation, sodium dihydrogen phosphate dihydrate and sodium hydrogen phosphate dihydrate for preparation of phosphate buffer (PB) (0.1 M, pH 7), and hydrogen peroxide (30%) were supplied by Sigma Aldrich. All solutions were prepared with ultra-pure water (18.2 MΩ cm) from a Sartorius Arium Comfort I system. ITO-coated glass was obtained from Biotain Crystal Co., Limited, with the following characteristics: resistance 6÷8 Ohm/sq, ITO coating thickness ~185 nm, transmittance >84%.

2.2. Fabrication of MnO_2 films on the surface of ITO.

Glass substrates were sonicated for 20 min in acetone, then in ethanol, washed with deionised water and dried with an Ar stream. A hole laser cut in Kapton tape defined the working area of the electrode of 0.69 cm^2. The electrochemical formation of the electrodes' functional layer was carried out by the methods of cyclic voltammetry (CV) with the region of scanned potentials from 1.0 V to 1.8 V. As electrolytes, we used water solutions of

0.005 M $MnSO_4$, 0.5 M Na_2SO_4 with pH 1 (the pH was adjusted by adding sulfuric acid) and added $CoSO_4$ in concentrations 0.01 M, 0.05 M and 0.1 M. The scan rate was 50 mV/s. All electrochemical experiments were performed using a potentiostat/galvanostat Bio-Logic SAS, model SP–300 in a conventional three-electrode glass cell. An Ag/AgCl/3M KCl electrode was used as reference and a Pt mesh as counter electrode. Each potential reported in this paper is given against Ag/AgCl/3M KCl at a laboratory temperature of 25 ± 1 °C. After electrodeposition, the dioxide films were dried at 60 °C or 90 °C in air for 15 h. Initial tests were performed with a Pt working electrode, which is a platinum disk with a diameter of 4 mm sealed in Teflon. The electrode surface was prepared as follows: mechanical polishing, rinsing with deionized water, and oxidation in a "piranha" solution (a mixture of concentrated sulfuric acid and hydrogen peroxide) for 5 min.

2.3. Analytical procedures for determination of H_2O_2 .

The electrochemical measurements were all carried out at temperature 37˚C (the temperature was maintained in a water bath). The cyclic voltammograms of the MnO_2/ITO electrode were scanned from 0.2–0.9 V in 0.1 M PB. The scan rate was 100 mV/s.

The catalytic activity of the MnO_2/ITO electrodes was determined using chronoamperometry in 0.1 M PB. The amperometric response was measured at an applied potential of 0.45 V vs Ag/AgCl/3M KCl during repeated injections of hydrogen peroxide.

2.4. Physical characterization of MnO_2/ITO electrodes.

The Microstructure and morphology of the MnO_2/ITO samples were investigated using a FEI Nova NanoSEM 450 scanning electron microscope.

X-ray photoelectron spectroscopic (XPS) measurements were performed using a PHI 5000 VersaProbe (ULVAC-PHI) spectrometer with monochromatic Al Kα radiation (h = 1486.6 eV) from an X-ray source operating at 100 µm spot size, 25 W and 15 kV. The high-resolution (HR) XPS spectra were collected with a hemispherical analyser at a pass energy of 117.4 and an energy step size of 0.1 eV. The X-ray beam was incident at the sample surface at an angle of 45° with respect to the surface normal, and the analyser axis was located at 45° with respect to the surface. The CasaXPS software was used to evaluate the XPS data. Deconvolution of all HR XPS spectra was performed using a Shirley background and a Gaussian peak shape with 30% Lorentzian character. The measured binding energies (BE) for individual elements were corrected in respect to the C1s carbon peak at 284.8 eV.

2.5. Quantum chemical calculations.

Quantum chemical modelling was performed using non-empirical methods of the WinGAMESS program [32–36]. Cluster systems were calculated using the spin-unrestricted Hartree-Fock method. The central metal atom was described by the ECP basis, and the ligand atoms by the 6-311G basis. The hybrid B3LYP method of density functional theory was used, which included five functionals: Becke, Slater, and Hartree-Fock exchange functionals, as well as LYP and VWN5 correlation functionals. In the simulation process, the studied ions were optimised in the environment of the first solvate shell and the energies of the optimised complexes were calculated. Then, the energies were refined taking into account solvation using the polarisation continuum model.

Since it makes sense to compare the electronic energies of different structures only if they contain the same type of atoms, when calculating the energy of complexes with different geometries of the first hydrate shell, we considered cluster systems of the composition $[Mn^{z+}(H_2O)_n]\ xH_2O$ under the condition that (n + x) = const. In this structure, n water molecules are directly connected to the central atom of the aqua complex, and the remaining x water molecules are at some distance, which excludes their chemical interaction with the metal ions. The cluster structure with the smallest sum of the energies of the metal aqua complex $[Mn^{z+(}H_2O)_n]$ and the energies x of the water molecules moved to the outer sphere was considered to be the most energetically favourable.

2.6 Microfluidic testing. Fabrication of the microfluidic system.

The PDMS chip is a T-shaped channel with two inputs. The channels are 250 microns high and 500 microns wide. Fluid manipulations were controlled by a Nemesys pump using dedicated computer software. The PDMS chip was connected to the ITO glass with a 2 mm-wide working electrode and with a graphite counter electrode at a distance of 2 mm from the working electrode. A silver chloride electrode was connected between them as a reference electrode. All measurements were carried out and recorded using a potentiostat, the characteristics of which are given in section 2.2.

3. Results and discussion.

3.1. Electrodeposition of doped Co^{2+} MnO_2 on ITO.

The formation of precipitates was carried out based on the experience of precipitation of pure manganese dioxide from a sulphate electrolyte (Fig. 1d).

In our previous work[37] the MnO_2 coating with the best catalytic and mechanical properties was formed by cyclic voltammetry (CV) in a solution with pH 1 and subsequently dried at 60 °C for 12 hours. We took these conditions as the basis for the current study. To obtain precipitates doped with Co^{2+} ions, sulphuric acid electrolytes were prepared with the addition of cobalt sulphate in concentrations from 0.01 M to 0.1 M. The quantities are significant, but it should be taken into account that it is unlikely that positively charged ions will move to the positively charged anode during electrophoresis; most likely, the doping mechanism is somewhat different.

Fig. 1a shows the CV dependence in a solution where only Co^{2+} ions are present. No reaction is observed on the platinum anode, which means that all the Ox-Red reactions in Figs. 1b-d are associated with the oxidation of the Mn^{2+} ions. Fig. 1b and 1c show the process of MnO_2 coating formation in the presence of 0.01 M and 0.1 M Co^{2+} ions in solutions, respectively. The influence of the doping agent on the deposition process can be analysed by comparison with the dependence in Fig.1d (precipitation of pure manganese dioxide). We observe a shift in the electrooxidation potential of Mn^{2+} by 0.5 V in the negative direction, which we associate with the influence of Co^{2+} ions. Based on the following studies, it can be assumed that Co^{2+} ions affect the structure and composition of the complex, in which divalent

manganese is oxidized at the anode. Perhaps it is as part of such complexes that cobalt is delivered to the surface of the electrode, where it is incorporated into the forming deposit.

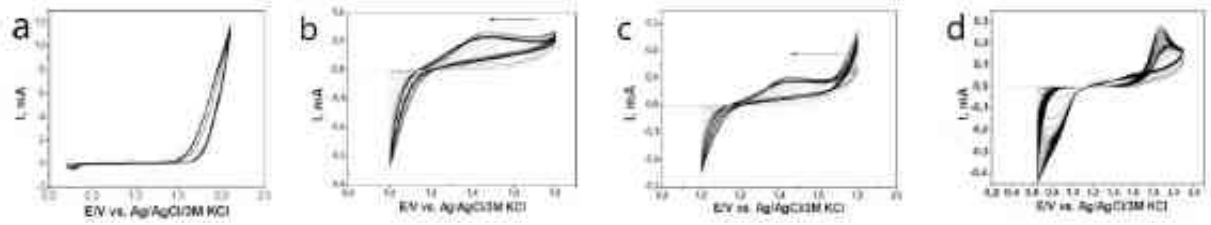

Fig.1. a) CV obtained by polarizing the Pt electrode in an electrolyte of the composition 0.5 M Na_2SO_4 +0.1 M $CoSO_4$, pH1; electrodeposition of MnO_2 by CV method from solution of 0.005 M $MnSO_4$ + 0.5 M Na_2SO_4 electrolyte, pH1 in the presence of b) 0.01 M $CoSO_4$, c) 0.1 M $CoSO_4$, d) without additives. Scan rate 50 mV/s

For catalytic studies, a set of sediments was prepared using different precipitation conditions. The differences are in the content of cobalt ions in the electrolyte and the number of CV cycles, resulting in different thicknesses of the sediment. The names of the electrodes used in the remainder of the article, with the corresponding deposition conditions, are summarised in Table 1.

Table 1. Conditions of precipitation formation.

Name of sample	Common conditions of electrodeposition Electrolyte: 0.5 M Na_2SO_4, 0.005 M $MnSO_4$, pH1, with the addition of $CoSO_4$	
	Concentration of Co^{2+}, M	Number of CV cycles
0.01Co_20	0.01	20
0.01Co_30	0.01	30
0.01Co_40	0.01	40
0.01Co_50	0.01	50
0.05Co_20	0.05	20
0.05Co_30	0.05	30
0.05Co_40	0.05	40
0.05Co_50	0.05	50
0.1Co_20	0.1	20
0.1Co_30	0.1	30
0.1Co_40	0.1	40
0.1Co_50	0.1	50
pH1_CV_60	-	30

3.2. Characterization of electrodes.

X-ray photoelectron spectroscopy (XPS) measurements were carried out to determine the presence of Co^{2+} ions in the sediment of MnO_2. We also investigated the influence of the electrolyte composition on the content and composition of the resulting catalysts from the point of view of manganese forms. The following three coatings were selected: 0.01Co_30; 0.05Co_30; 0.1Co_30 (the description of precipitation formation is given in section 3.1). The composition of electrolytes differed only in the concentration of cobalt ions.

The obtained XPS spectra are shown in Fig. 2. We used studies [38–41] that provide detailed descriptions of the interpretation of the XPS spectra of MnO_2 sediments. The Mn2p spectrum provides information that we indeed have a precipitate of manganese dioxide through the value of spin energy separation, which is equal to the distance between the $Mn2p_{3/2}$ and $Mn2p_{1/2}$ signals. The areas of the peaks at 641.9 eV and 644.9 eV of the $Mn2p_{3/2}$ signal allow us to calculate the ratio of the Mn^{+3} and Mn^{+4} forms. Particularly interesting results were obtained from the analysis of the O1s spectrum. We identify the peak at

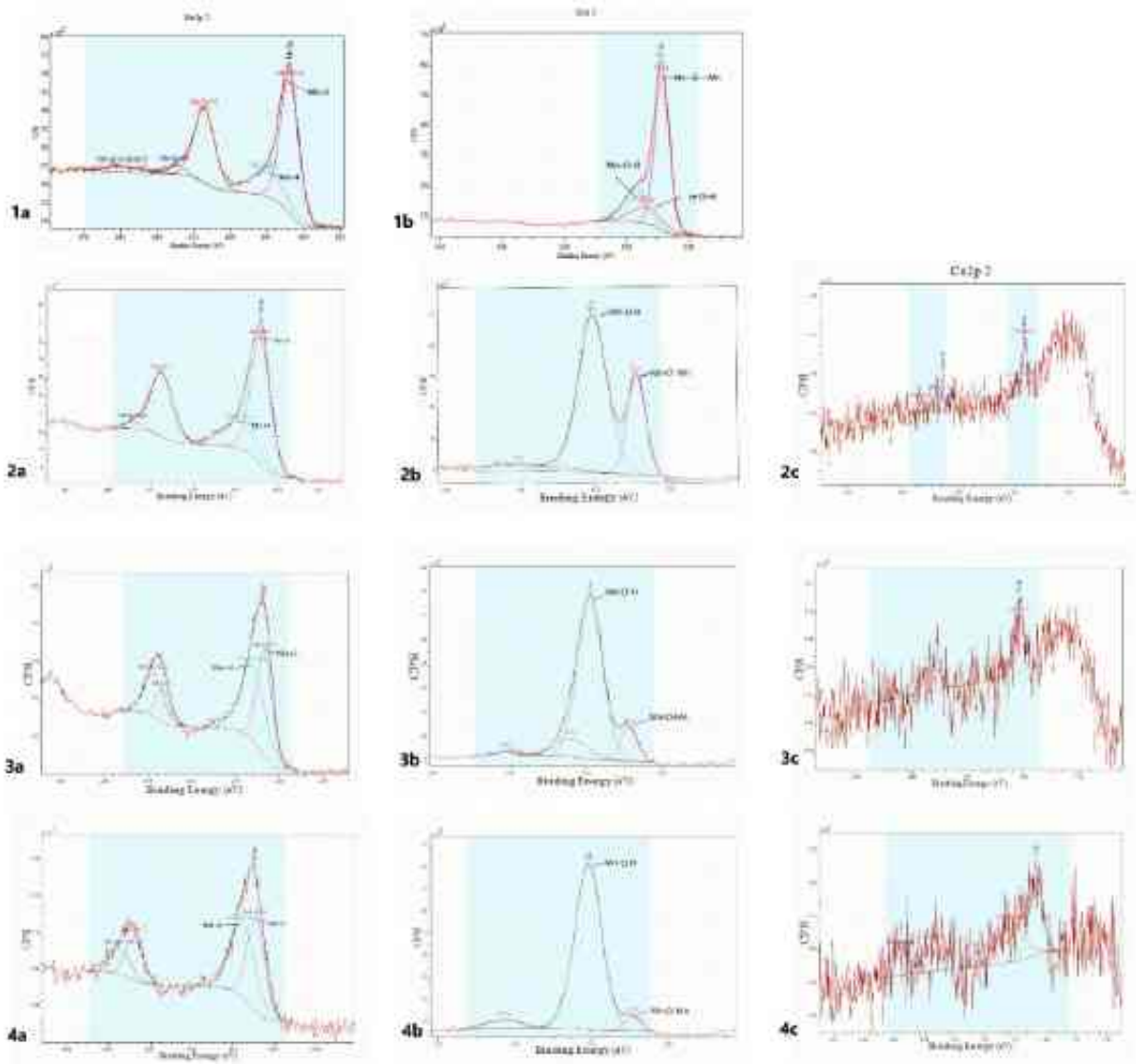

Fig. 2. Mn2p, O1s, Co2p XPS spectra of (1a, 1b) pH1_CV_60; (2a, 2b, 2c) 0.01Co_30; (3a, 3b, 3c) 0.05Co_30; (4a, 4b, 4c) 0.1Co_30. For details, see the main text

529.6 eV as the presence of Mn-O-Mn bonds, and the peak at 531.3 eV corresponds to the presence of Mn-O-H bonds. The Co2p2 spectrum confirms the presence of Co^{2+} ions in the resulting precipitates. The proportion of cobalt ions is presented as the content in the sediment relative to all manganese ions. The results are given in Table 2. We also added the results of XPS analysis of pure MnO_2, which was deposited under the same conditions. This way we can see the effect of doping on the catalyst composition.

Table 21 The XPS spectra interpretation.

Precipitate	**Mn2p spectrum, spin energy separation, eV**	**Mn^{3+}, %**	**Mn^{4+}, %**	**Mn-O-Mn, %**	**Mn-O-H, %**	**Co^{2+}, %**
Pure MnO_2	11.7	67.9	32.09	65.53	18.62	-
0.01Co_30	11.7	47	52.9	26.23	65.68	2.3
0.05Co_30	11.6	63.9	36	10.99	74.36	2.4
0.1Co_30	11.8	54.3	45.7	4.95	88.84	6.8

From the data in the table, we can conclude that Co^{2+} ions are indeed present in the structure of the formed MnO_2-based coating. However, their content does not linearly depend on the concentration in the solution. We see a sharp increase at 0.1 M Co^{2+} concentration in the electrolyte.

The ratio of Mn^{3+} / Mn^{4+} forms changes in the direction of increasing the content of manganese in its tetravalent form. The increase in catalytic activity due to the increase in the Mn^{+4} content agrees with the conclusions from our previous publication. [37] Also, the data shows that with the addition of Co^{2+} ions into the sediment, the amount of Mn-O-H bonds increases sharply. Such significant changes in the sediment composition can also influence the increase in the catalytic activity of the electrodes.

The morphology of the sediments were studied by scanning electron microscopy. Fig. 3 shows precipitates doped with Co^{2+}, electrodeposited in solutions with different cobalt ion contents. Images 3g and 3h show the morphology of pure MnO_2 and are given for comparison. All precipitates were formed during 30 cycles of CV at the same pH of the electrolyte and the same concentration of Mn^{2+} ions.

First of all, it is clear that the doped coatings are very similar. The structure is branched like the branches of trees. When compared with pure MnO_2, the structure is more branched, but the branches are smaller. We also observe an increase in the density of sediments; the structure of the ITO is not visible through the layer of manganese dioxide. At lower magnification we note the uniformity of the coating. We observe the integrity of the sediment, there are no cracks, which was typical for pure MnO_2.

When cobalt ions are added to the electrolyte, the resulting deposits become much denser, but the structure remains branched. The composition of the coating has undergone

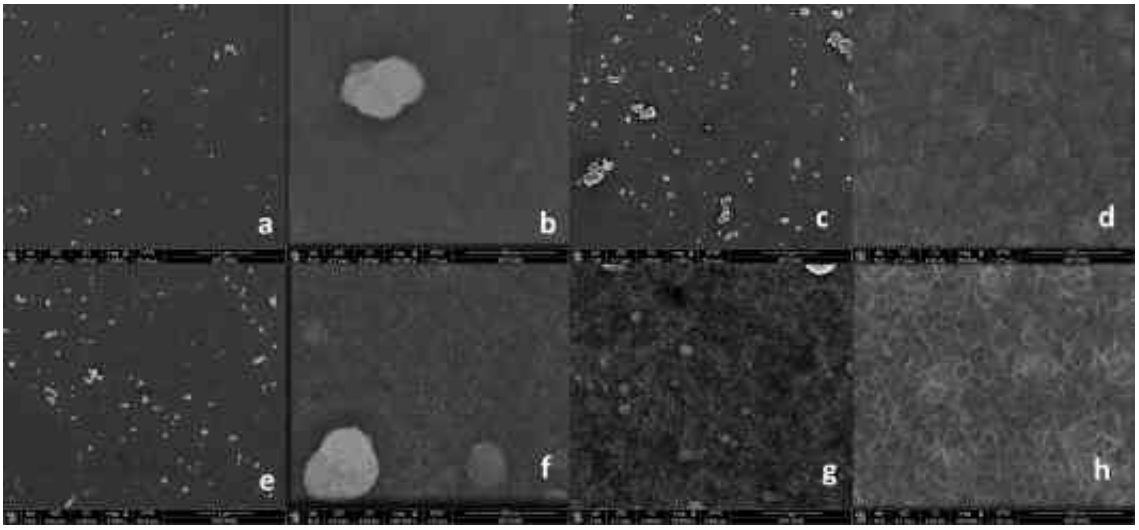

Fig. 3. SEM images of MnO_2 films deposited under conditions: (a, b) 0.01Co_30, (c, d) 0.05Co_30, (e, f) 0.1Co_30, (g, h) pH1_CV_60. For details, see the main text

significant changes. The ions Co^{2+} were found in the structure of all sediments. The effect on the structure of MnO_2 is also noticeable: the number of hydroxyl groups associated with manganese has sharply increased (Mn-O-H bonds).

3.3. Analytical procedure for the determination of H_2O_2

Based on convincing data from the literature [42,43], the mechanism of formation of an electrochemical signal during anodic polarisation of the working electrode is as follows. H_2O_2 decomposes into water and molecular oxygen when it comes into contact with MnO_2. The catalytic action is exerted by Mn^{4+}, which is reduced to Mn^{3+}. During anodic polarisation of the electrode, the Mn^{3+} will be electrochemically oxidized back to Mn^{4+}, which can be measured as a faradaic current. Interpretation of the data from the catalytic studies will be grounded in this theory.

The catalytic effect of the precipitate and the potentials at which it is observed were investigated by comparing voltammograms recorded in the presence and absence of H_2O_2 (Fig. 4). The cyclic voltammograms in the presence of H_2O_2 (Fig. 4(2)) show a higher current than CVs in the absence of hydrogen peroxide (Fig. 4(1)) even at low potentials. This means that even a low anodic polarisation will provide an analytical signal.

Chronoamperometry was chosen as the main method for studying the catalytic activity in determining H_2O_2 for a set of 12 electrodes. The method is indicative and convenient in interpretation. 0.45 V vs Ag/AgCl/3M KCl was chosen as a favourable potential at which the analytical signal is recorded. At this potential, we record sufficient catalytic activity, but avoid excess noise from the evolved gaseous products. Additionally, low values of electrode polarisation are desirable when studying biological objects, due to the presence of potentially interfering reactions.

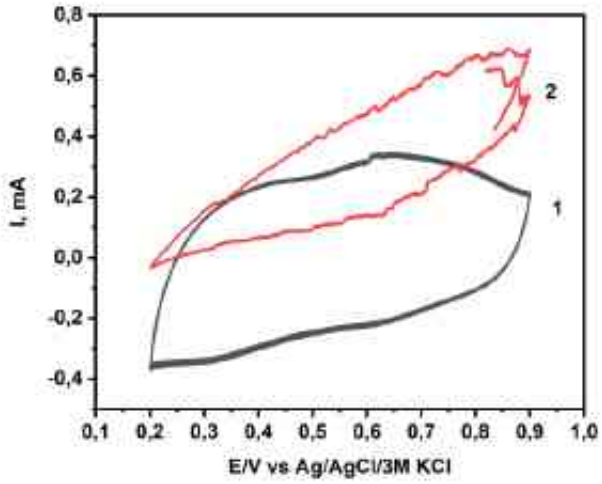

Fig.4. CVs of electrode 0.1Co_30 in the absence (1) and presence (2) of 2 mM H_2O_2 in PB. Scan rate 100 mV/s.

Fig. 5 shows the I-t dependences of all electrodes with H_2O_2 injections in such a way that the concentration of peroxide in the electrolyte changes stepwise according to the following scheme: 0.1 mM → 0.2 mM → 0.5 mM → 1 mM → 2 mM → 3 mM →…→ n mM. The high level of noise seen in Fig. 5 is due to the release of gaseous products from the decomposition of H_2O_2 while testing the electrodes, as described above.

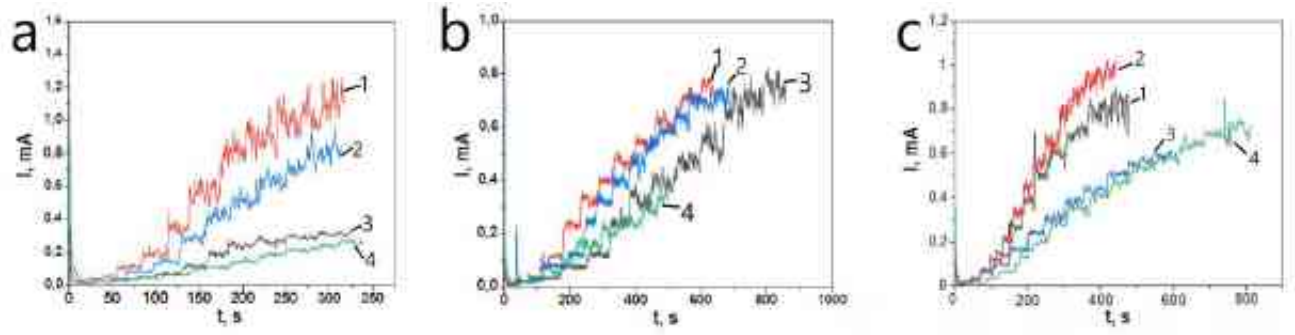

Fig.5. Amperometric I-t curves on successive injection of H_2O_2 into stirred PB at the applied potential of 0,45 V vs. Ag/AgCl/3M KCl of MnO_2 doped with Co^{2+} electrodes: (a1) 0.01Co_20, (a2) 0.01Co_30, (a3) 0.01Co_40, (a4) 0.01Co_50, (b1) 0.05Co_20, (b2) 0.05Co_30, (b3) 0.05Co_40, (b4) 0.05Co_50,(c1) 0.1Co_20, (c2) 0.1Co_30, (c3) 0.1Co_40, (c4) 0.1Co_50. Note that vertical scales are different.

For clarity, the results are divided into three groups: each figure (5a, 5b and 5c) shows chronoamperograms of electrodes formed with the same concentration of Co^{2+} ions and differ in sediment thickness. Thus, it is immediately clear that electrodes deposited with 20 to 30 CV cycles exhibit the highest activity. The activity of the catalysts decreases sharply at 40 and 50 CV cycles. This decrease in MnO_2 catalytic activity is a consequence of the relatively poor electrical conductivity of the material

The I-t dependencies of the best representatives of each group are converted into an amperometric response to H_2O_2 concentration and are compared with each other and with an electrode covered by a layer of pure MnO_2 (Fig.6).

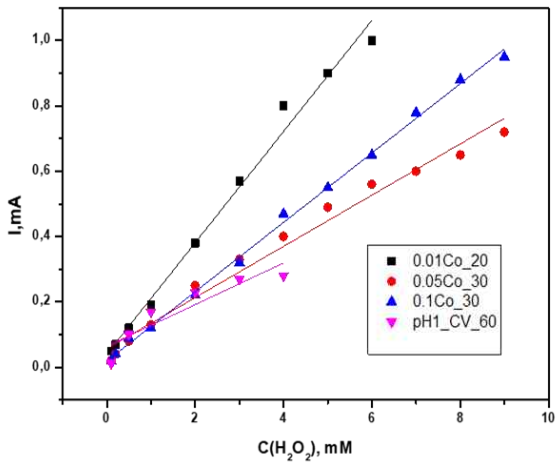

Fig.6. Relationship of the amperometric response vs. the H_2O_2 concentration, with data from Fig 5.

All catalysts doped with Co^{2+} ions show a sharp increase in the range of detectable H_2O_2 concentrations compared to pure MnO_2.

Another important parameter of such a dependence is its linearity. In this case, we have a calibration plot of electrocatalytic current versus H_2O_2 concentration. Pure MnO_2 shows a linear relationship with the concentration of H_2O_2 from 0.1 mM to 3 mM. Electrode 0.01Co_20 – from 0.1 mM to 4 mM, electrode 0.05Co_30 – from 0.1 mM to 6 mM, electrode 0.1Co_30 – from 0.1 mM to 9 mM. When selecting the electrode with the best performance, we distinguish 0.1Co_30 with the widest range of the calibration plot. Such a great improvement in the catalytic properties of the sediment, from the point of view of all the above studies, can be associated with a sharp increase in the Mn-O-H groups and their participation in the decomposition of hydrogen peroxide. We are going to consider changes in the electrode structure during the electrode transition. For this, we use the capabilities of quantum chemical modelling.

3.4. Quantum chemical computations.

The purpose of the calculations was to study the oxidation reaction of Mn^{3+} to Mn^{4+}, which is responsible for the electrocatalysis of the material. Section 2.5 provides references showing good correlation between calculated data and experimental data for Mn complexes.

As is known from previous studies [44] ,manganese dioxide contains Mn^{3+} in hydrolysed form. It is in these forms that we find the presence of the Mn-O-H bonds that attracted attention in the XPS study. All possible clusters were analysed and the actual charge

distributions in them were calculated, and the spatial particles were constructed. The results are shown in Table 3.

From Table 3, which shows the charge levels in trivalent manganese complexes, we can conclude that in reality, the Manganese atom does not carry a charge of +3, but rather the charge is redistributed among the oxygen-containing clusters around the central atom. Therefore, the hydrolysed form of Mn^{3+} is natural. And it is precisely in such complexes that a large presence of Mn-O-H bonds is observed.

The next stage of calculations is the analysis of energy changes associated with the transition of an electron during the oxidation of
trivalent manganese to the tetravalent state and back. This is actually the reaction that provides electrocatalysis. Possible reactions of electron transition from hydrolysed trivalent manganese are presented in Table 4. There you can see the energy characteristics of electron transition and the calculated standard electrode potentials of these reactions

Table 3. Distribution of charges on manganese atoms and ligands in clusters $[Mn\ (OH)_x(H_2O)_n]^{z+}\ (H_2O)_m$ and $[Mn\ O(OH)(H_2O)_2] + (H_2O)_2$.

Clusters	q(Mn)	q(ΣOH)	q(O)	q(ΣH_2O)
$[Mn(OH)(H_2O)_5]^{2+}$	+1,937	-0,362	-	+0,425
$[Mn(OH)_2(H_2O)_4]^{+}$	+1,751	-0,996	-	+0,244
$[Mn(OH)_3(H_2O)_2]^{0}(H_2O)$	+1,500	-1,607	-	+0,127
$[MnO(OH)(H_2O)_2]^{0}(H_2O)_2$	+1,342	-0,561	-0,829	+0,048
$[Mn(OH)(H_2O)_5]^{3+}$	+2,121	+0,076	-	+0,801
$[Mn(OH)_2(H_2O)_4]^{2+}$	+1,819	-0,341	-	+0,522
$[Mn(OH)_3(H_2O)_2]^{+}(H_2O)$	+1,589	-0,832	-	+0,244
$[MnO(OH)(H_2O)_2]^{+}(H_2O)_2$	+1,617	-0,414	-0,469	+0,266

Table 4. Values of standard Red-Ox potentials of one-electron oxidation of hydrolysed forms of manganese(III) aquacomplexes

№	Reaction	ΔE, kJ/mol	ϕ^0, V (Standard Hydrogen Potential)
1	$[Mn(OH)(H_2O)_5]^{2+} = [Mn(OH)(H_2O)_5]^{3+} + e$	775,791	2,90
2	$[Mn(OH)_2(H_2O)_4]^{+} = [Mn(OH)_2(H_2O)_4]^{2+} + e$	692,902	2,15
3	$[Mn(OH)_3(H_2O)_3]^{0} = [Mn(OH)_3(H_2O)_2]^{+}(H_2O) + e$	577,246	1,11
4	$[Mn(OH)_3(H_2O)_2]^{0}(H_2O) = [Mn(OH)_3(H_2O)_2]^{+}(H_2O) + e$	602,132	1,33
5	$[MnO(OH)(H_2O)_2]^{0}(H_2O)_2 = [MnO(OH)(H_2O)_2]^{+}(H_2O)_2 + e$	512,457	0,53

Most likely reaction number 5 occurs. The standard electrode transition potential is very low, which correlates with our catalytic measurements. We conclude that trivalent manganese in the electrolytic film MnO_x is present in the form of the compound $[MnO(OH)(H_2O)_2]$. Removing water and the OH group from the structure showed that such a particle could not be calculated, which demonstrates the importance of the presence of these groups in the structure of the sediment. Calculations also indicate that other particle geometries are possible, but the electrode transition potential increases sharply in this case. In Fig.7 shows the structures of $[MnO(OH)(H_2O)_2]$ in the original and, accordingly, in the oxidized state.

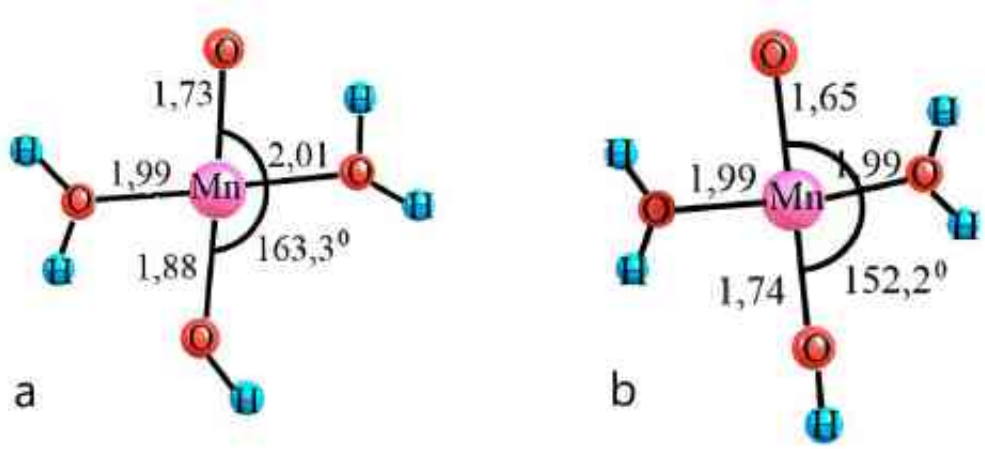

Fig. 7. Spatial structure of particles: a - $[MnO(OH)(H_2O)_2]^0$;b - $[MnO(OH)(H_2O)_2]^+$

As can be seen, the removal of an electron from $[MnO(OH)(H_2O)_2]$ does not lead to a significant reorganization of its structure. The Mn-OH bonds remain unchanged and stable: the internuclear distances in them are 1.99 Å and 2.01 Å in the molecular form and 1.99 Å and 1.99 Å in the ionized form. A slight displacement of Manganese and Oxygen nuclei is observed only in Mn-O and Mn-O-H bonds. In the molecular form, they are 1.73 Å and 1.88 Å, respectively, and in the ionized form, 1.65 Å and 1.74 Å. The valence angle O-Mn-O-H also changes little: from 163.30 in the molecular form to 152.20 in the ionized form. The above listed indicates the absence of major structural and chemical transformations in the redox system $[MnO(OH)(H_2O)_2]$/ $[MnO(OH)(H_2O)_2]^+$. which makes it possible to use in objects in which rapid charge cycling is assumed.

Thus, it can be concluded that the more Mn-O-H bonds present in the precipitate, the greater the probability of the formation of a hydrolysed structure of trivalent manganese $[MnO(OH)(H_2O)_2]$ a certain geometry. Then the reactions of the Mn^{3+}/ Mn^{4+} transformations will occur easily and quickly at minimal electrode polarization potentials. This is reflected in the excellent catalytic performance of the MnO_2 electrode.

3.5. Measurements in a microfluidic system.

The developed MnO_2-based electrode with the best performance was implemented as a working electrode in an amperometric microfluidic device for determining the concentration

of H_2O_2 in a solution. The creation of the microfluidic cell is described in detail in Section 2.6 and is also visually represented in the Fig.8. The T-shaped channels and two inlets allow manipulation with two working solutions. One of them was PB with H_2O_2 of a given concentration, and the second was pure PB, which was used to wash the channels between receiving signals. In this system, with a very small working electrode area and microamounts of electrolyte, the amplification of the analytical signal is achieved due to the hydrodynamic effect of analyte delivery. H_2O_2 concentrations of the order of μM were measured. However, one drawback of the electrode was noticed. Despite the low speed of liquid movement (20 μl/s), the MnO_2 layer was quickly washed off during measurements. This is because Mn^{3+} compounds are soluble in water. Thus, despite the high sensitivity, the signal would not reach a steady-state, and a calibration curve could not be established.

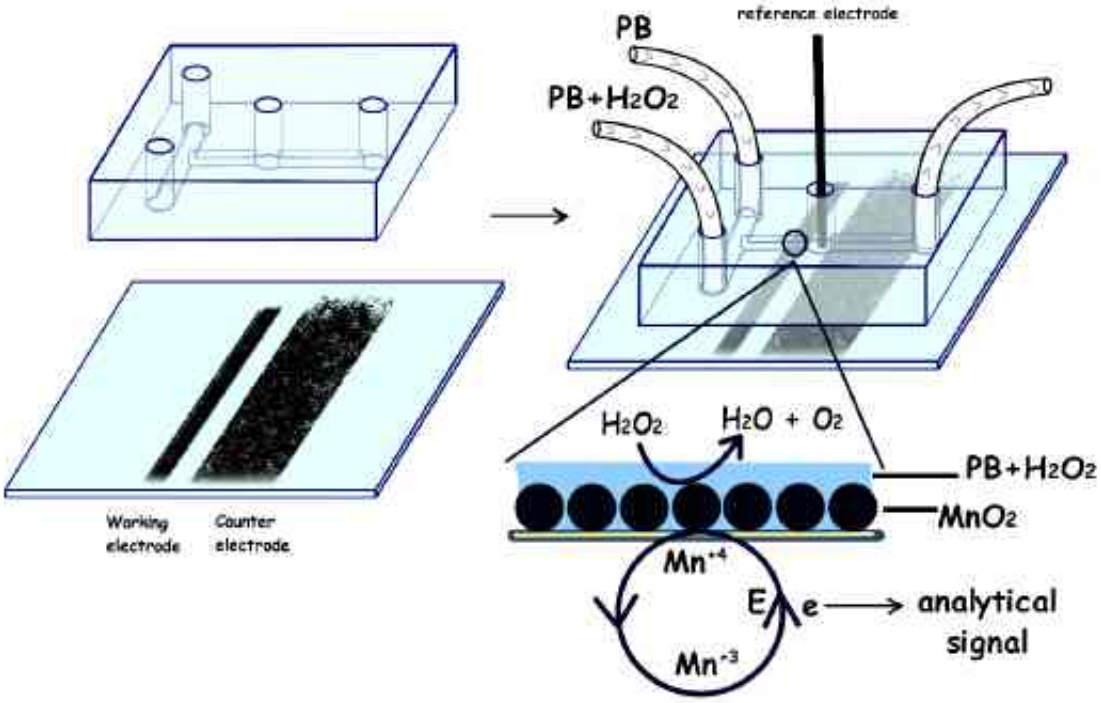

Fig. 8. Schematic illustration of the microfluidic cell with MnO_2-based working electrode.

Therefore, an alternative scheme for working with MnO_2 electrodes needed to be developed. We stop the flow of electrolyte with H_2O_2 when it hits the electrode and measure the charge (q) passing through the electrode while hydrogen peroxide decomposes. This charge is related to the amount of decomposed H_2O_2 through Faraday's first law:

$$m = M*q/F*n,$$

where m is the mass of the manganese that took part in the Ox-Red reaction, proportional to the decomposed hydrogen peroxide,

M is the molar mass manganese dioxide, q is the total electric charge passed through the electrolyte (in Coulombs), n is the number of electrons involved in the reaction and F is Faraday's constant, approximately 96,485 Coulombs per mole.

For specific electrolysis M, F, n are constants; thus, the value of q is equivalent to m. In the case of constant-current electrolysis,

$$q = It$$

Where I is the current, t is the time of process.

The Fig.9 shows the signal that we received. The PB solution flows through the channel to point 1. From point 1 to point 2 a solution containing hydrogen peroxide flows. From point 2 to point 3, the movement of solutions in the system stops. From point 3, pure PB flows and washes the cell channels, and the process can be repeated. The charge (q) is measured as the area under the chronoamperogram curve from point 2 to point 3.

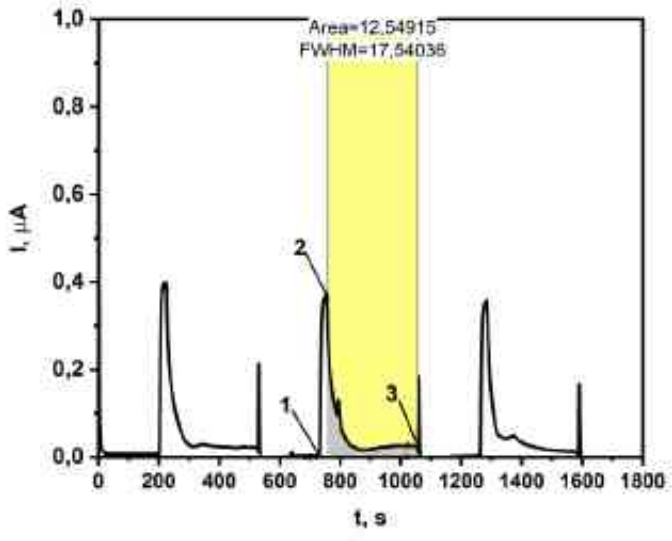

Fig.9. I-t dependence obtained in the microfluidic system. Analyte 20 μM H_2O_2 in 0.1 M PB

Based on our experience, time periods should be selected in accordance with the object of study. In this investigation, the optimal program was as follows: PB flow for 200 s, then inclusion of H_2O_2 in phosphate buffer for 30 s, stopping the liquids for the reaction to proceed for 300 s. The flow rate is always 20 μl /s. In the process of developing the methodology, 4 electrodes were used and 6 concentrations of hydrogen peroxide were measured on them: 5 μM, 10 μM, 15 μM, 20 μM, 30 μM, 40 μM. As a result, calibration curves are considered as the dependence of the charge recorded on the working electrode on the concentration of H_2O_2.

The electrodes were evaluated in terms of the reproducibility of successive measurements on them. Referring to Figure 9, then the first measurement spans from 200 s to 500 s, the second measurement is from 750 s to 1050 s, and the third measurement is from 1300 s to 1600 s. Results for one of the electrodes are shown in Fig. 10. The first measurement can often be unreproducible as shown by a large variation and missing data points.

Dependencies 2 and 3 are quite reproducible and have a correlation coefficient of about 0.99. When processing the results. For this reason, the second measurement was used in the analyses.

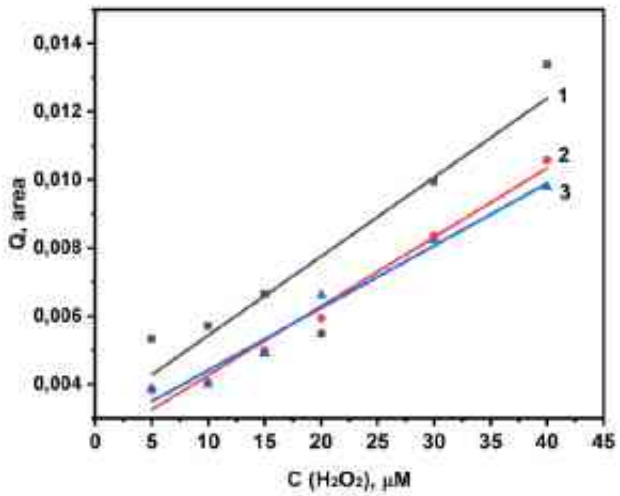

Fig.10. Dependence of charge recorded on the working electrode on the concentration of H_2O_2 : 1- first measurement, 2- second measurement, 3- third measurement.

Fig. 11 shows the calibration curves for four electrodes. Several series of measurements (6 concentrations of hydrogen peroxide) were carried out on all electrodes; the figure shows an example of two series of measurements for the fourth electrode.

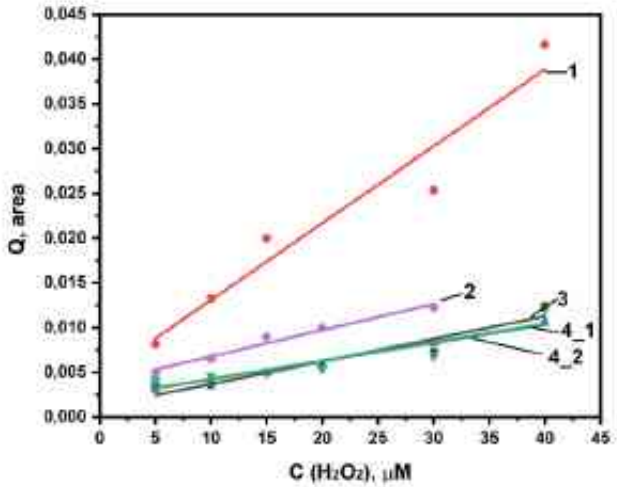

Fig.11. Dependence of charge recorded on the working electrode on the concentration of H_2O_2: 1 – first electrode, 2 – second electrode, 3 – third electrode, 4_1 –first measurements on the fourth electrode, 4_2 - second measurements on the fourth electrode

All electrodes showed the possibility of constructing a calibration curve with a correlation coefficient from 0.96 to 0.99. However, we note that the reproducibility between electrodes is insufficient. In effect, this means that before using the electrode, a separate

calibration should be carried out. But, as the examples 4_1 and 4_2 show, very high reproducibility is seen from measurement to measurement, which implies that this is a manufacturing issue, rather than a fundamental limitation of the MnO_2 electrodes.

This study showed that a highly sensitive electrode for a microfluidic cell was developed for quantitative measurement of H_2O_2 at concentrations as low as 5 µM.

4. Conclusion

Doping MnO_2 with Co^{2+} ions is a simple procedure, but it significantly improves the catalytic properties of this catalyst. We combined physical methods for studying the composition of sediments and their morphology with quantum chemical modelling of the basic catalytic reaction. The results indicate that due to the increase in the hydrolysed forms of manganese (Mn-O-H bonds), the range of determination of H_2O_2 concentrations relative to pure MnO_2 increases several times. In systematic catalytic studies in a macroscopic cell with stirred solution, the electrode 0.1Co_30 with the highest content of Co^{2+} ions and Mn-O-H bonds in the composition showed mechanical strength, a stable range of determination of hydrogen peroxide concentrations from 0.1 mM to 9 mM. For comparison, the range of detectable H_2O_2 concentrations when using an electrode with pure MnO_2 is from 0.1 mM to 3 mM.

Testing the 0.1Co_30 sample with the best characteristics in a microfluidic system showed the high sensitivity of the catalyst. Stable determination of H_2O_2 concentration 5 µM. The measurement mechanism we have developed takes into account the characteristics of the electrode composition to ensure stability of the electrode during repeated measurements. and ensures sufficiently long-term operation with a large number of analysed samples.

We would like to add that after use the MnO_2 layer is easily removed and the ITO base can be used again. Our experience shows that ITO glass can be use this way for at least 6 months with a reprecipitation frequency of once every 1-2 weeks. This makes the analysis inexpensive and environmentally friendly.

Acknowledgements:
This work was supported by the Norway Grants 2014-2021 via the National Centre for Research and Development (NOR/POLNOR/UPTURN_UA/0060/2019).

Data availability
Electrochemical data have been made available at the RepOD repository, doi: 10.18150/PUHR5I

There are no conflicts to declare.

References

1. Valencia, L. *et al.* A new microfluidic method enabling the generation of multi-layered tissues-on-chips using skin cells as a proof of concept. *Sci. Rep.* **11**, 13160 (2021).
2. Gale, B. K. *et al.* A Review of Current Methods in Microfluidic Device Fabrication and Future Commercialization Prospects. *Inventions* **3**, 60 (2018).
3. Preetam, S. *et al.* Emergence of microfluidics for next generation biomedical devices. *Biosens. Bioelectron. X* **10**, 100106 (2022).
4. Zhang, D. *et al.* Microfluidic Technology: A New Strategy for Controllable Synthesis of Metal Nanomaterials. *ChemElectroChem* **12**, e202400666 (2025).
5. Kling, A. *et al.* Electrochemical Microfluidic Platform for Simultaneous Multi-analyte Detection. *Procedia Eng.* **120**, 916–919 (2015).
6. Qiang, L., Vaddiraju, S., Rusling, J. F. & Papadimitrakopoulos, F. Highly sensitive and reusable Pt-black microfluidic electrodes for long-term electrochemical sensing. *Biosens. Bioelectron.* **26**, 682–688 (2010).
7. Kang, S. & Davis, J. J. Leveraging microfluidic confinement to boost assay sensitivity and selectivity. *Chem. Sci.* **16**, 6965–6974 (2025).
8. Veal, E. A., Day, A. M. & Morgan, B. A. Hydrogen Peroxide Sensing and Signaling. *Mol. Cell* **26**, 1–14 (2007).
9. Neill, S. Hydrogen peroxide signalling. *Curr. Opin. Plant Biol.* **5**, 388–395 (2002).
10. Sujitha, A. S., Aswathy, M. R., Ragupathy, L. & Painuly, D. A free-standing, flexible electrospun nanofibrous membrane composed of gold nanoclusters for the detection of hydrogen peroxide and its real-time application in cancer detection. *Sens. Actuators B Chem.* **426**, 137078 (2025).
11. Jawad, S. E. Z. *et al.* Ascorbic acid-immobilized zinc selenide for electrochemical monitoring of hydrogen peroxide in liver cancer samples. *Sci. Rep.* **15**, 237 (2025).
12. Ali, T. *et al.* Generation of Hydrogen Peroxide in Cancer Cells: Advancing Therapeutic Approaches for Cancer Treatment. *Cancers* **16**, 2171 (2024).
13. Kacem, H. *et al.* Modification of the microstructure of the CERN- CLEAR-VHEE beam at the picosecond scale modifies ZFE morphogenesis but has no impact on hydrogen peroxide production. *Radiother. Oncol.* **209**, 110942 (2025).
14. Ahmad, T. *et al.* Recent Advances in Electrochemical Sensing of Hydrogen Peroxide (H2O2) Released from Cancer Cells. *Nanomaterials* **12**, 1475 (2022).
15. La Favor, J. D. & Burnett, A. L. A microdialysis method to measure in vivo hydrogen peroxide and superoxide in various rodent tissues. *Methods* **109**, 131–140 (2016).
16. Pravda, J. Hydrogen peroxide and disease: towards a unified system of pathogenesis and therapeutics. *Mol. Med.* **26**, 41 (2020).

17. Huang, C. *et al.* Hydrogen peroxide responsive covalent cyclodextrin framework for targeted therapy of inflammatory bowel disease. *Carbohydr. Polym.* **285**, 119252 (2022).
18. Song, Y. *et al.* Roles of Hydrogen Peroxide in Thyroid Physiology and Disease. *J. Clin. Endocrinol. Metab.* **92**, 3764–3773 (2007).
19. Guo, S., Wen, D., Dong, S. & Wang, E. Gold nanowire assembling architecture for H2O2 electrochemical sensor. *Talanta* **77**, 1510–1517 (2009).
20. Dong, W., Ren, Y., Bai, Z., Yang, Y. & Chen, Q. Fabrication of hexahedral Au-Pd/graphene nanocomposites biosensor and its application in cancer cell H2O2 detection. *Bioelectrochemistry* **128**, 274–282 (2019).
21. Delvaux, M., Walcarius, A. & Demoustier-Champagne, S. Electrocatalytic H2O2 amperometric detection using gold nanotube electrode ensembles. *Anal. Chim. Acta* **525**, 221–230 (2004).
22. He, W. *et al.* Intrinsic catalytic activity of Au nanoparticles with respect to hydrogen peroxide decomposition and superoxide scavenging. *Biomaterials* **34**, 765–773 (2013).
23. Sun, Y. *et al.* Laser-induced formation of Au/Pt nanorods with peroxidase mimicking and SERS enhancement properties for application to the colorimetric determination of H2O2. *Microchim. Acta* **185**, 445 (2018).
24. Ye, Y., Sun, X., Zhang, Y., Han, X. & Sun, X. A novel cell-based electrochemical biosensor based on MnO2 catalysis for antioxidant activity evaluation of anthocyanins. *Biosens. Bioelectron.* **202**, 113990 (2022).
25. Li, L. *et al.* A novel nonenzymatic hydrogen peroxide sensor based on MnO2/graphene oxide nanocomposite. *Talanta* **82**, 1637–1641 (2010).
26. Uddin, B. *et al.* Enhancing the photocatalytic properties of nickel oxide nanoparticles via iron doping: Efficient degradation of eosin yellow dye. *Chem. Phys. Impact* **10**, 100798 (2025).
27. Thanh, T. D. *et al.* Iron oxide nanoparticles synthesized by coprecipitation method: Impacts of zinc doping and surface functionalization by polyvinylpyrrolidone on the magnetic properties and heating efficiency. *Ceram. Int.* **51**, 1448–1455 (2025).
28. Asaldoust, F., Mabhouti, K., Jafari, A. & Taleb-Abbasi, M. Structural, magnetic, and optical characteristics of undoped and chromium, iron, cobalt, copper, and zinc doped nickel oxide nanopowders. *Sci. Rep.* **15**, 1088 (2025).
29. Xian, C. *et al.* Cobalt-catalyzed reversible deposition/dissolution of MnO2 for enhancing the long-cycle stability of aqueous Zn-Mn batteries. *Chem. Eng. J.* **512**, 162576 (2025).
30. Chen, X. *et al.* Oxygen Vacancy-Rich Cobalt-Doped MnO_2 Nanorods for Zn Ion Batteries. *ACS Appl. Mater. Interfaces* **17**, 12074–12084 (2025).
31. Zudina, L., Sokolsky, G., Chumak, V. & Haiuk, N. OER/ORR parameters of Fe2+ and Co2+-doped manganese dioxide electrode materials. *Mater. Today Proc.* **62**, 7759–7766 (2022).

32. Seredyuk, V. A. & Vargalyuk, V. F. Estimation of reliability of quantum-chemical calculations of electronic transitions in aqua complexes of transition metals. *Russ. J. Electrochem.* **44**, 1105–1112 (2008).

33. Schmidt, M. W. *et al.* General atomic and molecular electronic structure system. *J. Comput. Chem.* **14**, 1347–1363 (1993).

34. Szafran, M., Karelson, M. M., Katritzky, A. R., Koput, J. & Zerner, M. C. Reconsideration of solvent effects calculated by semiempirical quantum chemical methods. *J. Comput. Chem.* **14**, 371–377 (1993).

35. Cammi, R. & Tomasi, J. Remarks on the use of the apparent surface charges (ASC) methods in solvation problems: Iterative versus matrix-inversion procedures and the renormalization of the apparent charges. *J. Comput. Chem.* **16**, 1449–1458 (1995).

36. Sakiyama, H., Oshima, M., Suzuki, S. & Nishida, Y. Several Molecular Orbital Computations for a Dinuclear Nickel(II) Complex. *J. Comput. Chem. Jpn.* **8**, 87–92 (2009).

37. Poltavets, V., Krawczyk, M., Maslak, G., Abraimova, O. & Jönsson-Niedziółka, M. Formation of MnO_2 -coated ITO electrodes with high catalytic activity for enzymatic glucose detection. *Dalton Trans.* **52**, 13769–13780 (2023).

38. Jeong, J.-H., Park, J. W., Lee, D. W., Baughman, R. H. & Kim, S. J. Electrodeposition of α-MnO2/γ-MnO2 on Carbon Nanotube for Yarn Supercapacitor. *Sci. Rep.* **9**, 11271 (2019).

39. Nesbitt, H. W. & Banerjee, D. Interpretation of XPS Mn(2p) spectra of Mn oxyhydroxides and constraints on the mechanism of MnO_2 precipitation. *Am. Mineral.* **83**, 305–315 (1998).

40. Biesinger, M. C. *et al.* Resolving surface chemical states in XPS analysis of first row transition metals, oxides and hydroxides: Cr, Mn, Fe, Co and Ni. *Appl. Surf. Sci.* **257**, 2717–2730 (2011).

41. Audi, A. A. & Sherwood, P. M. A. Valence-band x-ray photoelectron spectroscopic studies of manganese and its oxides interpreted by cluster and band structure calculations. *Surf. Interface Anal.* **33**, 274–282 (2002).

42. Beyene, N. W. *et al.* (Bio)sensors based on manganese dioxide-modified carbon substrates: retrospections, further improvements and applications. *Talanta* **64**, 1151–1159 (2004).

43. Turkusic, E. *et al.* Amperometric determination of bonded glucose with an MnO2 and glucose oxidase bulk-modified screen-printed electrode using flow-injection analysis. *Talanta* **65**, 559–564 (2005).

44. Poltavets, V. V., Vargalyuk, V. F., Seredyuk, V. A. & Shevchenko, L. V. The mechanism of electrooxidation of Mn2+ ions. *J. Chem. Technol.* **26**, 1–11 (2018).